sustainability

MDPI

Article

Long Term Quantification of Climate and Land Cover Change Impacts on Streamflow in an Alpine River Catchment, Northwestern China

Zhenliang Yin, Qi Feng *, Linshan Yang, Xiaohu Wen, Jianhua Si and Songbing Zou

Key Laboratory of Ecohydrology of Inland River Basin, Northwest Institute of Eco-Environment and Resources, Chinese Academy of Sciences, Lanzhou 730000, China; yinzhenliang@lzb.ac.cn (Z.Y.); yanglsh08@lzb.ac.cn (L.Y.); xhwen@lzb.ac.cn (X.W.); jianhuas@lzb.ac.cn (J.S.); zousongbing@lzb.ac.cn (S.Z.)

* Correspondence: qifeng@lzb.ac.cn; Tel.: +86-931-4967-089

Received: 11 April 2017; Accepted: 19 July 2017; Published: 20 July 2017

Abstract: Quantifying the long term impacts of climate and land cover change on streamflow is of great important for sustainable water resources management in inland river basins. The Soil and Water Assessment Tool (SWAT) model was employed to simulate the streamflow in the upper reaches of Heihe River Basin, northwestern China, over the last half century. The Sequential Uncertainty Fitting algorithm (SUFI-2) was selected to calibrate and validate the SWAT model. The results showed that both Nash-Sutcliffe efficiency (*NSE*) and determination coefficient (R^2) were over 0.93 for calibration and validation periods, the percent bias (*PBIAS*) of the two periods were—3.47% and 1.81%, respectively. The precipitation, average, maximum, and minimum air temperature were all showing increasing trends, with 14.87 mm/10 years, 0.30 °C/10 years, 0.27 °C/10 year, and 0.37 °C/10 years, respectively. Runoff coefficient has increased from 0.36 (averaged during 1964 to 1988) to 0.39 (averaged during 1989 to 2013). Based on the SWAT simulation, we quantified the contribution of climate and land cover change to streamflow change, indicated that the land cover change had a positive impact on river discharge by increasing 7.12% of the streamflow during 1964 to 1988, and climate change contributed 14.08% for the streamflow increasing over last 50 years. Meanwhile, the climate change impact was intensive after 2000s. The increasing of streamflow contributed to the increasing of total streamflow by 64.1% for cold season (November to following March) and 35.9% for warm season (April to October). The results provide some references for dealing with climate and land cover change in an inland river basin for water resource management and planning.

Keywords: streamflow; climate change; land cover change; Heihe River Basin; SWAT

1. Introduction

Water resource pressure has become one of the important factors that affect social and economic sustainable development and ecosystem security [1,2]. It is widely recognized that climate and land cover changes are two important factors affecting water resources availability in water-constrained regions [3–6]. Affected by the changing environment, climate-related water issues such as flood and drought occur frequently and result in serious consequences in these regions [7,8]. Therefore, the impacts of climate change and land cover change on water resources availability are of great concern for sustainable development, especially in arid and semi-arid inland river basins [9,10].

Climate change alters the hydrological cycle in a direct way by influencing the distribution of precipitation, variations of evapotranspiration and streamflow [11,12]. Meanwhile, climate change is always coupled with the land cover change [13]. Climate and land cover changes result in more complex interactive relationships among precipitation changes, temperature changes, and runoff

changes [14]. Quantitatively assessing the impact of climate and land cover changes on water resource availability is a significant issue for hydrological science [10,15,16]. Today, high-quality land cover types can usually be acquired via remote sensing technology developed after the 1980s. Hydrological models, such as the SWAT [17,18], TOPMODEL [19], and VIC [20], are commonly used to study the effect of climate change on the hydrological cycle. Based on physical mechanisms, hydrological models offer a framework for conceptualizing and investigating the relationships between climate, land cover, and hydrological processes in various categories of time and space [21,22]. Hydrological models consider the hydrological processes and their interactions with the environment [13,21,22].

There are numerous studies that investigate the impacts of climate and land use/cover changes on water resources availability based on hydrological model [10,23–26], but few address how climate change impacts streamflow at a long time period and what role land cover change plays in runoff change. These issues remain to be resolved [16,27]. In order to fully understand the interaction between the hydrological processes and changing environment, we need to apply a method to distinguish the climate change impact from the impact of land cover change on streamflow changes. However, due to the scarcity for the land cover maps before the 1980s, it is impossible to drive the hydrological model using observed land cover types as input parameter for many regions, especially for the mountainous regions of inland river basins over a long term period. Here, we come up with a new method trying to understand the climate change impact on streamflow over a relative long time period. Based on change point analysis [6,22], the streamflow is divided into two phases, the previous phase (baseline) and the latter phase (effect period). During the latter phase, the land cover map can be collected by remote sensing methods. Thus, the hydrological model can be calibrated using observed streamflow, climate condition, and land cover map in the latter phase, and then the calibrated parameters are entirely used to simulate runoff in the previous phase. The difference between the observed and simulated runoff for the previous phase accounts for the impact of land cover change on streamflow. The difference between the simulated runoff for latter phase and the previous phase is considered to quantify the impact of climate change on streamflow. Thus, we can distinguish the contribution of climate change from the land cover change in order to understand the impacts of the changing environment.

The mountainous region of an inland river basin is one of the most sensitive areas for climate change [28–30]. Thus, we chose the upper reaches of the Heihe River Basin (HRB) as our study area. We have described the basic situation in our previous study [31]. There are several studies simulating hydrological processes in the HRB [1,17,29,32–35]. However, there has been little work done to assess the impact of the changing environment on streamflow of the upper mountainous watershed over a long time period. Yang et al. [36] have identified the separate impacts of climate and land cover changes on hydrological processes in upper stream of HRB based on the obtained climate data and land use/cover change data from 1981 to 2010. However, their study only focused on conditions over 30 years; long-term study on the climate and land cover change impacts still remains to be addressed. In this study, we prolong the time series in order to quantify the impacts of climate and land cover changes on streamflow in a longer time series. We selected the SWAT model to facilitate this research based on its wide use. In order to know what changes have happened for the hydro-meteorological processes in this area, we choose several variables—precipitation, days of precipitation, air temperature (average, minimum, and maximum), and streamflow—to analysis the variation trends.

2. Materials

2.1. Study Area

The Yingluoxia watershed (YLX watershed) is located at the upper reaches of HRB covering an area of 10,018 km^2 (Figure 1). It is the main region for streamflow generation, contributing about 90% of the water resources of the Heihe main stream. The Yingluoxia (YLX) hydrological station is located in the outlet of the watershed and monitors the runoff of the watershed. The climate in the watershed is characterized as cold and dry in winter and hot and wet in summer. The annual

precipitation tends to decrease from east to west and increase from 200 mm to 700 mm with the increasing altitude. Detailed information about the YLX watershed can be found in Yin et al. [31] and Cheng et al. [37].

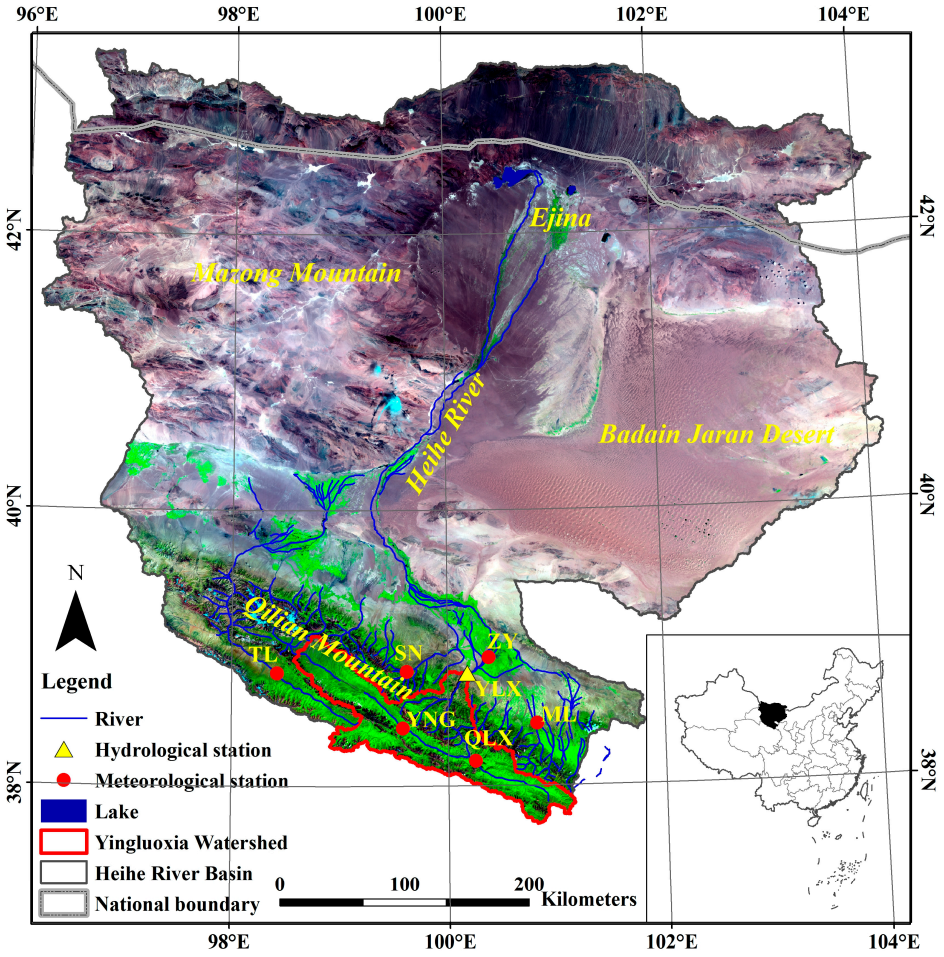

Figure 1. Location of the Heihe River Basin, the meteorological station, and hydrological station in and surrounding the Yingluoxia (YLX) Watershed.

2.2. Data Availability

The ASTER GDEM, with a resolution of 30 m, was used as the digital elevation model (DEM) data in this study, as shown in Figure 2a. The hydrological and meteorological observation data were all acquired from the portal of http://westdc.westgis.ac.cn. The land cover map was obtained with the type groups, including alpine meadow (51.1% of the YLX watershed), grassland (14.2%), forest land (18.8%), bare land (15.4%), and glacier (0.5%). The land cover map in this study was interpreted from the remote sensing image in 2001 by the Institute of Botany of the Chinese Academy of Sciences. The land cover map is shown in Figure 2b. The soil map (scale 1:1,000,000) comes from the China Soil Scientific Database (CSSD), as shown in Figure 2c. Related main soil properties were processed as described in our previous study [31].

Daily climate data, including precipitation, maximum and minimum air temperature, average wind speed, relative humidity, and sunshine duration, were obtained from the records of the six meteorological stations in Figure 1. Monthly river flow data was obtained from the YLX hydrological station for the observation period from 1961 to 2013.

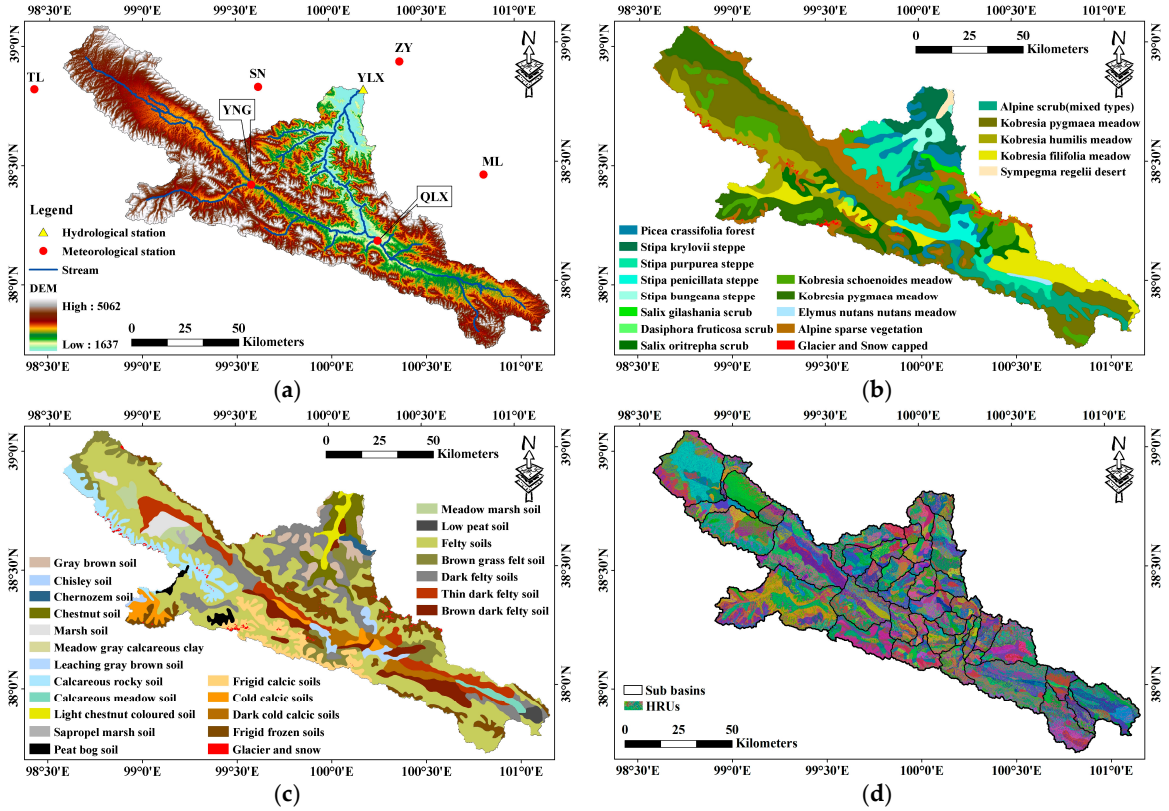

Figure 2. The DEM (**a**), land cover (**b**), soil type (**c**), sub basins, and Hydrologic Response Units (**d**) of the YLX watershed.

3. Methodologies

3.1. Distinguishing the Impacts of Climate and Land Cover Changes

We considered that the observed streamflow series reflect the interactive relationship between climate and land cover changes. Due to lack of the available land cover maps from the 1960s to the 1980s, it is hard to achieve good performance when we simulate the hydrological processes using the SWAT model. Based on the change point analysis [38], both temperature and precipitation in Northwest China underwent abrupt change around 1987. Considering the length of time series, we took 1989 as a demarcation point. Some studies also indicate that climate change shifted around 1989 [39,40]. Thus, we divided the streamflow into two phases, the previous phase (1964 to 1988, 25 years) and the latter phase (1989 to 2013, 25 years). During the latter phase, we collected the land cover map [41] as described in the data availability section and calibrated and validated the SWAT model. Then, the calibrated model was used to simulate runoff in the previous phase. The real streamflow (observed streamflow) was the reflection of interactions between climate change and land cover change. In the previous phase SWAT simulation, we used the calibrated SWAT model expecting to get a perfect result; however, we used the changed land cover map (constructed in 2001) to drive the model, so the simulated runoff could be considered as the result affected by the land cover change. The difference between observed and simulated runoff in the previous phase could be considered as the impact of land cover change as shown in the left part of the flowchart (Figure 3). We used the same land cover map in the previous phase simulation and latter phase simulation; however, the climate was changing, so the differences between the simulated runoff of the two phases were considered to quantify the impact of climate change on streamflow. Finally, we distinguished the impact of climate change from land cover change. The flowchart is shown in Figure 3.

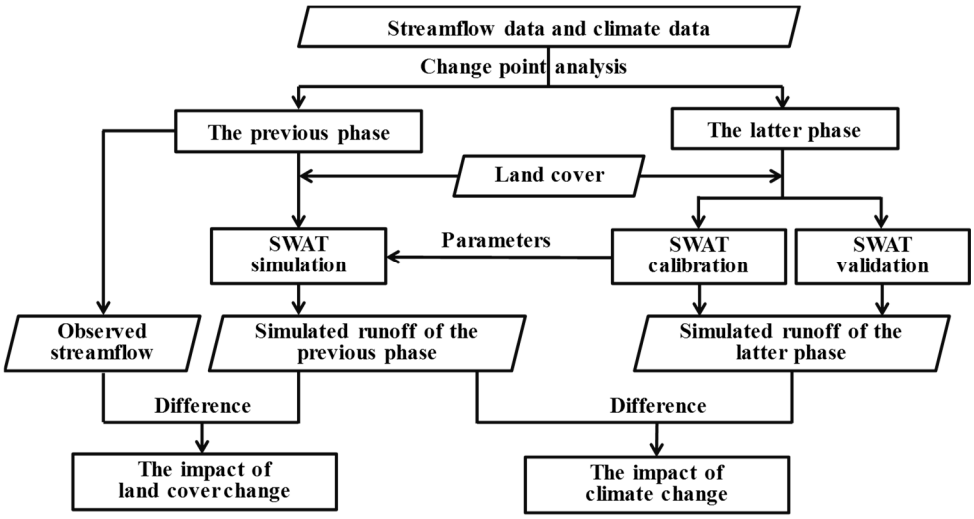

Figure 3. The flowchart for distinguishing the impacts of climate and land cover changes.

3.2. Soil and Water Assessment Tool (SWAT) Model and Model Setup

The SWAT model is a physically based hydrological model developed by the United States Department of Agriculture [42]. It is effective in modeling hydrological components and process responses such as climate change, land cover change, and different watershed management at variable time scales with semi-distributed treatment for large river basins [43]. In this study, we simulated the snow and glacier melt by using an elevation banded temperature index method—the detail can be found in reference [31].

The hydrologic cycle as simulated by SWAT is based on the water balance equation,

$$SW_t = SW_0 + \sum_{i=1}^{t} (R_{day} - Q_s - E_a - w_{seep} - Q_g) \quad (1)$$

where SW_t is the final soil water content (mm), SW_0 is the initial soil water content on day i (mm), t is the time (days), R_{day} is the amount of precipitation on day i (mm), Q_s is the amount of surface runoff on day i (mm), E_a is the amount of ET on day i (mm), w_{seep} is the amount of water entering the vadose zone from the soil profile on day i (mm), and Q_g is the amount of return flow on day i (mm).

According our previous study [31], the model setup included four steps: watershed discretization and sub-basin characteristics derivation, HRU definition, parameter sensitivity analysis, and model calibration and validation. In the watershed discretization, the YLX watershed was discretized into 43 sub-basins as shown in Figure 2d. In the HRU definition, the 43 sub-basins were delineated into 2650 HRUs on the basis of land cover type, soil type, and terrain features, as shown in Figure 2d. In this step, the land cover related parameters (such as maximum potential leaf area index, canopy height, root depth, optimal (base) temperature for plant growth, and harvest index) were read from the SWAT model attribute database and were then written into every HRU attribute file. The land cover–related parameters stored in the SWAT model attribute database were obtained from field investigation and measurement. The soil-related parameters were also read from the attribute database and were then written into every HRU attribute file. During the simulation, the SWAT model read the HRU parameters from the HRU attribute file to calculate water balance of the HRU.

3.3. Model Calibration and Confirmation Analysis

In this study, calibration and uncertainty analyses were performed by SUFI-2 [44]. In SUFI-2, 95PPU (95% prediction uncertainty) was calculated at the 2.5% and 97.5% levels of the cumulative

distribution of output variables. Based on the sensitivity analysis and our previous study [35,45], 15 parameters were chosen, whose final fitted parameter value are shown in Table 1.

Table 1. Parameters involved in the calibration procedure and final fitted values.

Parameter [1]	Description	Parameter Range	Fitted Value
r_CN2.mgt	Initial SCS runoff curve number for moisture condition II	−0.4~0.2	−0.225
v_ALPHA_BF.gw	Base flow alpha factor (days)	0.0~0.5	0.25
v_GW_DELAY.gw	Groundwater delay time (days)	90.0~180.0	165.0
v_GWQMN.gw	Threshold depth of water in the shallow aquifer required for return flow to occur (mm)	0.0~2.0	1.0
v_GW_REVAP.gw	Groundwater 'rewap' coefficient	0.0~0.2	0.033
v_ESCO.hru	Soil evaporation compensation factor	0.5~0.9	0.70
v_CH_N2.rte	Manning's '*n*' value for the main channel	0.0~0.3	0.05
v_CH_K2.rte	Effective hydraulic conductivity in main channel alluvium (mm/h)	5.0~40.0	10.83
v_ALPHA_BNK.rte	Base flow alpha factor for bank storage	0.0~1.0	0.50
r_SOL_AWC.sol	Available water capacity of the soil layer (mm H_2O/mm soil)	−0.2~0.4	−0.10
r_SOL_K.sol	Saturated hydraulic conductivity (mm/h)	−0.8~0.8	−0.53
v_SFTMP.bsn	Snowfall temperature (°C)	−2.0~1.0	−1.5
v_SMFMN.bsn	Melt factor on December 21 (mm H_2O/°C-day)	0~10.0	3.5
v_SMFMX.bsn	Melt factor on June 21 (mm H_2O/°C-day)	0~10.0	7.5
v_TLPAS.sub	Temperature lapse rate (°C/km)	−8.0~−4.0	−5.5

[1] r_: parameter value is multiplied by (1 + a given value) or relative change; v_: parameter value is replaced by given value or absolute change.

The Nash-Sutcliffe Efficiency (*NSE*), the determination coefficient (R^2), and the percent bias (*PBIAS*) are frequently used measures in hydrologic modeling studies [45], which are calculated as,

$$NSE = 1 - \frac{\sum_{i=1}^{n}(O_i - P_i)^2}{\sum_{i=1}^{n}(O_i - O_{avg})^2} \quad (2)$$

$$R^2 = \frac{\left(\sum_{i=1}^{n}(O_i - O_{avg})(P_i - P_{avg})\right)^2}{\sum_{i=1}^{n}(O_i - O_{avg})^2 \sum_{i=1}^{n}(P_i - P_{avg})^2} \quad (3)$$

$$PBIAS = \frac{\sum_{i=1}^{n}(P_i - O_i)}{\sum_{i=1}^{n} O_i} \times 100\% \quad (4)$$

in which, P_i is the simulated streamflow, O_i is the observed streamflow at time step i, respectively, whereas P_{avg} and O_{avg} are the average simulated and observed streamflow values in time period 1, 2, . . . , n.

3.4. Mann-Kendall Trend Test

The Mann-Kendall (M-K) test, based on the work of Mann [46] and Kendall [47], was used to assess the influence of a trend base on non-parametric testing. The M-K test is widely used for trend analysis in hydrology and climatology [37,48–50].

The change levels of meteorological variables in this study were estimated by the application of the Sen Slope method. This technique calculates the slope as a change in measurement correlated with units of temporal change. It offers the advantages of allowing for missing data, avoiding assumptions on distribution of data, and averting the effects of gross data errors and outliers [51]. The Sen Method can eliminate the consequences of missing data or anomalous trends by using the median of the series of slopes as the judgmental foundation. The expression is given by,

$$\beta = Median \frac{(x_j - x_i)}{(j - i)}, \forall j > i \quad (5)$$

where $1 < j < i < n$. the estimator β is the median over all combinations of record pairs for the whole data set. A positive value of β indicates an "increasing trend," and a negative value indicates a "decreasing trend."

4. Results and Discussion

4.1. Model Performance

According to the distinguish method described in Section 3.1, we divided the streamflow into two phases: the Impact Testing phase (IT phase, 1964–1988) and the model Calibration and Validation phase (CV phase, 1989–2013). In this study, we divided the Calibration and Validation phases into three sub-periods: the first sub-period (1986 to 1988) was set as warming up period, the second sub-period (1989 to 2000) was used to calibrate the model, and the last sub-period (2001 to 2013) was applied to validate the model with the observed streamflow data at Yinluoxia station as target.

We estimated the performance of the modeling results such as *NSE*, *R*, and *PBIAS* for different periods, which can be seen in Table 2. The results of the SWAT simulation was fairly in accordance with the observed river flow at the monthly time scale with an *NSE* of 0.93 during calibration and validation periods (Figure 4), which is a very good performance according to the classification standard [45]. Moreover, the high values of R^2 reflect high correlation between the simulated results and the observed data, as shown in Figure 5. Even though the values of *PBIAS* indicated that the average tendency of the simulated data underestimated the observed data a little, the general performance was still acceptable.

Table 2. Values of *NSE*, *R*, and *PBIAS* in different study periods.

Period	*NSE*	R^2	*PBIAS* (%)
Calibration (1989–2000)	0.93	0.95	−3.47
Validation (2001–2013)	0.93	0.93	1.81
The CV phase (1989–2013)	0.93	0.93	−0.59
The IT phase (1964–1988)	0.92	0.94	7.12

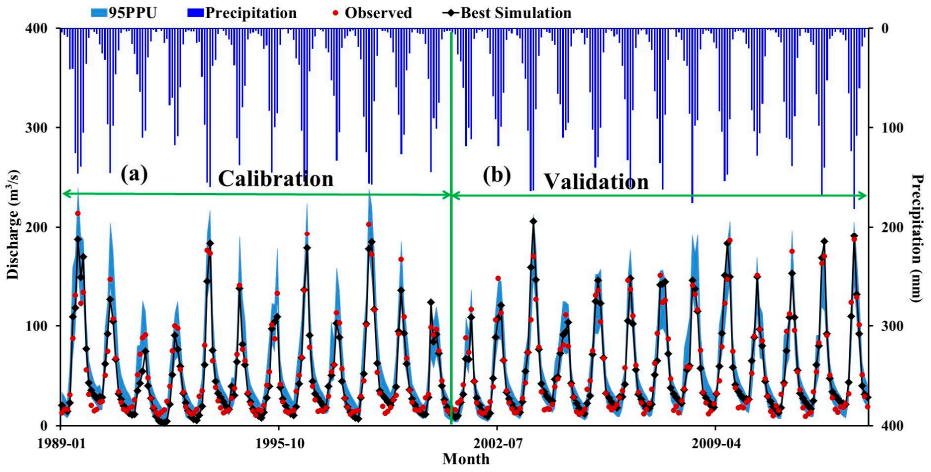

Figure 4. Monthly observed and simulated river discharge in the YLX hydrological station during the calibration period (**a**) and the validation period (**b**) with the uncertainties of simulation and monthly precipitation of the YLX watershed.

Moreover, the 95PPU model results are shown in Figure 4, wherein the shaded region show the uncertainty of the model parameter without accounting for the uncertainties of the model structure and model input. The results revealed that SWAT is an effective tool in simulating the hydrological processes in the upper stream of HRB, with very satisfactory accuracy by the *P*-factor of 86% and *R*-factor of 0.72 in the calibration period.

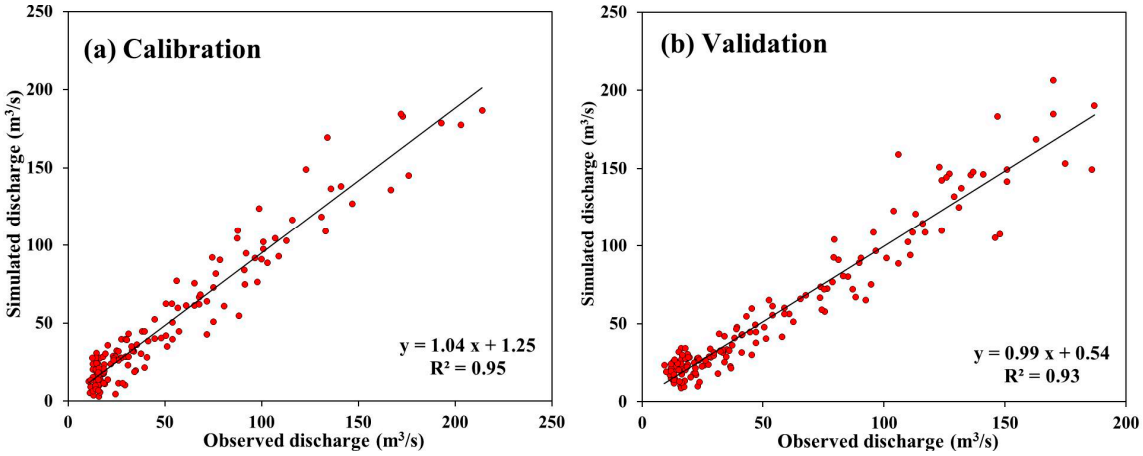

Figure 5. Scatter plots the observed and simulated streamflow for the calibration (**a**) and the validation (**b**) periods in the study area.

4.2. The Change in Hydro-Meteorological Variables

We employed precipitation, days of precipitation, air temperature (average, minimum, and maximum), and streamflow data to represent the changes in hydro-meteorological processes. A precipitation day here is defined as a day with more than 1 mm of precipitation. Figure 6 and Table 3 show that great changes happened among the hydro-meteorological variables over the last 50 years. The annual precipitation increased significantly, by 1.49 mm/year for β value during the period ($p < 0.05$). Days of precipitation in the year increased by 0.132 day/year for β value with non-significance. The monthly changes in precipitation and days of precipitation in the month increased more in warm seasons than in cold seasons. The annual average, minimum, and maximum air temperatures increased

significantly ($p < 0.01$). The increasing trends of precipitation and temperature were in accordance with the results of QLX meteorological station [52]. The increasing magnitude of minimum air temperature was largest among the three air temperature variables. Compare to their monthly changes, the increase magnitudes in cold months were larger than that in warm months. The annual streamflow also increased significantly by 0.937 mm/year for β value ($p < 0.01$). The monthly streamflow increased in all months with significant magnitudes, except in May and July. It should be noted that the streamflow was increasing obviously in wet season due to the large variation of precipitation. The results of this section were partly demonstrated in our previous study [31].

Table 3. Annual statistics of hydro-meteorological series, their average, trends, and significance during 1964–2013.

Variable	Average	Slope of Regression Line (year^{-1})	M-K Test	β (year^{-1})	Significance
Precipitation (mm)	420.65	1.542	2.52	1.487	<0.05
Days of precipitation (days)	75.32	0.134	1.42	0.132	-
Average air temperature (°C)	−2.83	0.030	4.82	0.030	<0.01
Minimum air temperature (°C)	−10.17	0.039	5.50	0.037	<0.01
Maximum air temperature (°C)	6.58	0.026	3.84	0.027	<0.01
Streamflow (mm)	160.28	0.914	3.92	0.937	<0.01

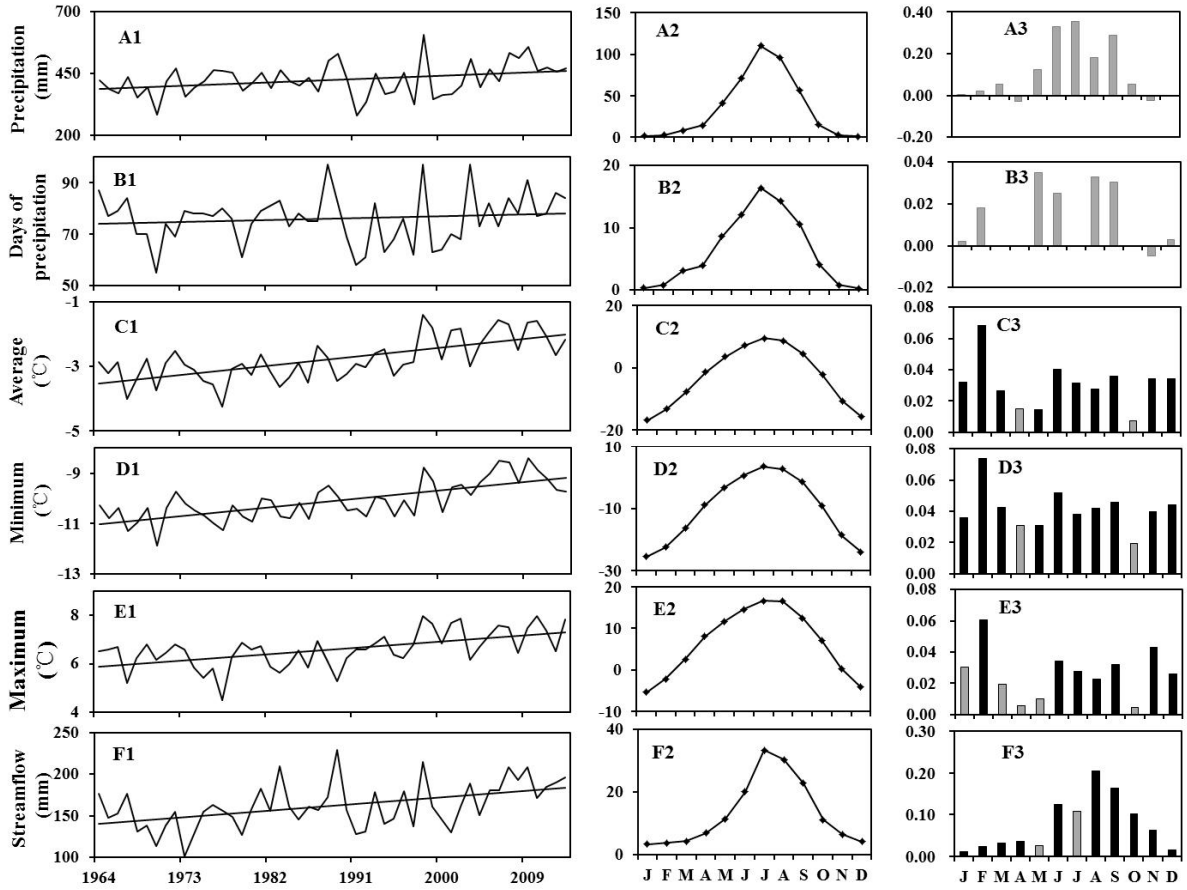

Figure 6. Information about the variables: (**A**) precipitation, (**B**) number of days of precipitation, (**C**) average air temperature, (**D**) minimum air temperature, (**E**) maximum air temperature, and (**F**) streamflow at YLX station. Left panel (**A1**–**F1**): annual average. Middle panel (**A2**–**F2**): monthly average. Right panel (**A3**–**F3**): monthly distribution of variation magnitudes of β value for each variable, black bar represent significance at 0.05 and gray bar represent not significant.

Figure 7 shows the correlativity of accumulated precipitation and streamflow in two periods. Compare to the two periods of scatter plots, we can clearly find that the rainfall-runoff relationship has been changed. For the same precipitation, the runoff yield for the period after 1989 was larger than that for the period before 1989. This means the runoff coefficient has increased during the entire period, while the runoff coefficient has changed from 0.36 (averaged during 1964 to 1988) to 0.39 (averaged during 1989 to 2013). However, what caused these changes? What were the impacts of climate and land cover changes on the streamflow? These subjects will be emphasized in the following sections.

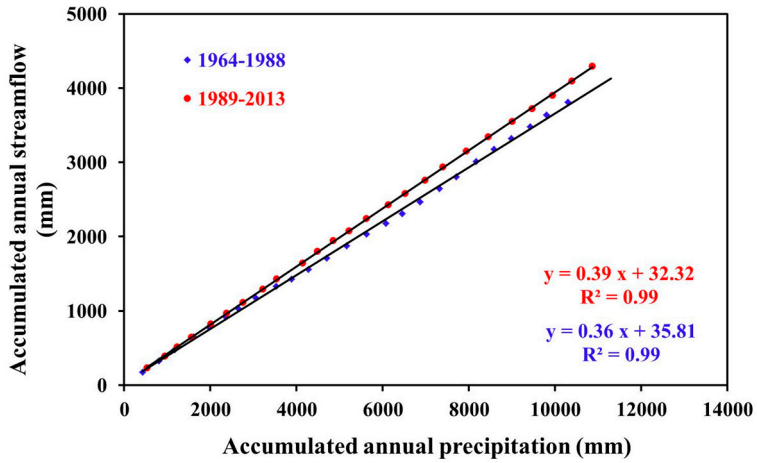

Figure 7. Scatter plots between accumulated annual precipitation and streamflow.

4.3. The Effects of Land Cover and Climate Change on Streamflow

4.3.1. Identifing the Effects of Land Cover Change on Streamflow

As described in previous section, we divided the study period into the IT phase and the CV phase. During the CV phase, we calibrated and validated SWAT model using observed streamflow, climate condition, and land cover map, and then the calibrated parameters were entirely used to simulate runoff in the IT phase. In this study, we reran the calibrated SWAT model in the IT phase using the current land cover map. Because the model was calibrated during the CV phase, the simulated streamflow in IT phase was considered as the results of land cover changes. Meanwhile, the observed streamflow in the IT phase was considered to be the result before the land cover changes. Therefore, the differences (simulated streamflow minus observed streamflow) between the observed and simulated streamflow for the IT phase were regarded as the impacts of land cover change on streamflow.

Figure 8 showed the differences between the observed and simulated streamflow during the IT phase and the CV phase. Compared to the simulated streamflow in CV phase, there was a great different between the simulated and observed streamflows in the IT phase. These differences reflected the impact of land cover change on river discharge. The differences for the river discharge (bottom box in Figure 8) were almost above zero in the IT phase. This indicated that the land cover change had a positive impact on river discharge. According to the model performance of the IT phase, the value of *NSE* and R^2 were 0.92 and 0.94, respectively, which indicated that the performance was perfect. However, the *PBIAS* was 7.12%, which meant that the simulation streamflow was higher than the observed streamflow (Table 2). Meanwhile, the PBIAS of −0.59% in the CV phase demonstrated that the bias caused by the model was almost negligible; thus, we regarded the PBIAS (7.12%) in the IT phase was induced by the impact of the land cover change. Figure 9 also reflects the positive effect of land cover change, although this impact was not obvious, which reflects the small change in land cover.

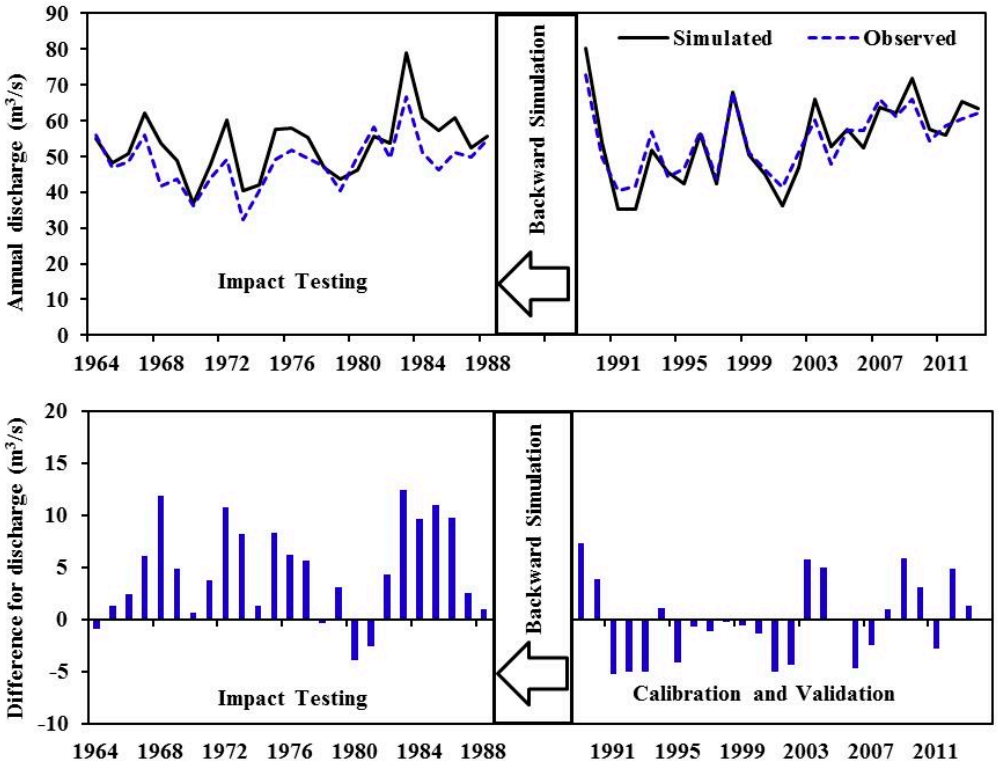

Figure 8. The observed and simulated river discharge from 1964 to 2013 (**top box**) and the differences between simulated and observed river discharge (**bottom box**).

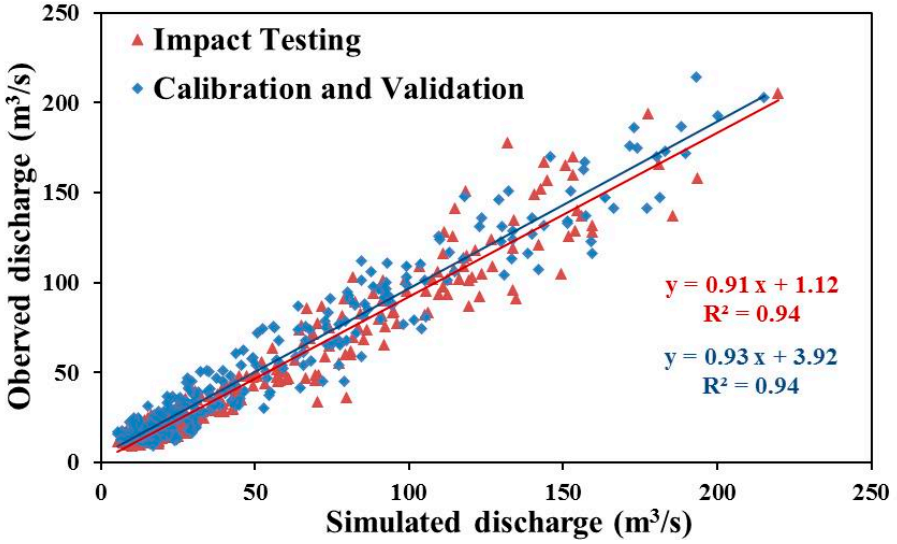

Figure 9. Scatter plots of simulated and observed river discharge in impact testing and calibration and validation period.

4.3.2. Quantifying Climate Change Contribution to Streamflow

The observed streamflow was coupled with the interaction of climate and land cover. In this case study, we simulated the streamflow over the last 50 years, assuming a changing climate and constant land cover. In order to eliminate the impacts of land cover changes on streamflow, we chose the simulated river discharge series, instead of the observed discharge series, to assess the contribution of climate change to streamflow. The average of decadal simulated precipitation (PCP), average

temperature (ta), and streamflow (R) were calculated as shown in Table 4. The average temperature was continuously increasing in every decade except the 1970s. Compared to the values in 1960s, the precipitation and streamflow decreased in the 1970s and the 1990s by 10.90 and 12.35, and 13.56 mm and 15.66 mm, respectively. The precipitation and streamflow both increased in the 1980s and after 2000. It should be noted that streamflow in the 2010s increased more obviously, with a value of 23.40 mm compare to the streamflow, than in any other decade before the 2010s. This indicates that the intensive influence of climate change on streamflow in the 2010s was more obvious than in any other decades from the 1960s onward.

The variation of streamflow was consistent with precipitation: both decreased in the 1970s and 1990s and increased in the 1980s and after 2000, which illustrates that the change to streamflow was mainly impacted by precipitation change. However, when the precipitation increased by 20.79 mm and 17.84 mm in the 1980s and 2010s, the streamflow increased by 22.30 mm and 23.40 mm, respectively, which demonstrates that the change of streamflow was also impacted by temperate change. According to Wu et al. [32], temperature warming induced the increase of snowmelt and glacier melting, consequently increasing the streamflow. Therefore, without considering the impact of land cover changes, the streamflow change was affected by precipitation change (rising) and temperature change (rising). According to our pervious study, the runoff coefficient was sensitive to precipitation and not to temperature [31]. We can see from the Table 4, compare to the 1960s, without considering land cover change impacts, the streamflow due to climate change decreased in the 1970s and 1990s by 8.11% and 9.39%, and increased in the 1980s, 2000s, and 2010s by 13.35%, 4.32%, and 14.01%, respectively. Overall the streamflow increasing due to climate change by 14.08% of total streamflow over the last 50 years, in agreement with the results of Wu et al. [53] and Zhang et al. [17]. The latest study also confirmed that the climate dominate the streamflow effects more significantly in the upper stream of the Heihe River rather than land cover change [36].

Table 4. Impacts of climate change to streamflow during the 1960s to the 2010s.

Decade	PCP (mm)	ta (°C)	R (mm)	PCP Change (mm)	ta Change (°C)	R Change (mm)	PCP (%)	ta (%)	R (%)
1960s	510.37	−1.55	167.10	-	-	-	-	-	-
1970s	499.47	−1.66	153.54	−10.90	−0.11	−13.56	−2.14	−7.10	−8.11
1980s	531.16	−1.53	189.40	20.79	0.02	22.30	4.07	1.29	13.35
1990s	498.02	−1.05	151.44	−12.35	0.50	−15.66	−2.42	32.26	−9.39
2000s	522.06	−0.46	174.31	11.69	1.09	7.21	2.29	70.32	4.32
2010s	528.21	−0.42	190.50	17.84	1.13	23.40	3.50	72.90	14.01

Figure 10 shows decadal changes of monthly precipitation, average temperature, and streamflow compared to values from the 1960s. The changes of monthly precipitation distributed unevenly within the year that were mainly increased from June to September, except for a sharp decrease in September in the 1990s, and mainly decreased in April, May, October, and November. Most of the monthly average temperatures increased, except for decreases from March to May. We have already discussed that the streamflow change was an interaction of precipitation change and temperature change without considering land cover change. It was the same in the monthly scale: the decreasing precipitation in April and May and decreasing temperature from March to May resulted in the streamflow decreasing from April to June. In addition, the increasing precipitation from July to September was accompanied by the rising temperature from June to September, which caused the streamflow rise from July to September. The abrupt reduction of precipitation in September in the 1990s caused the increase of streamflow.

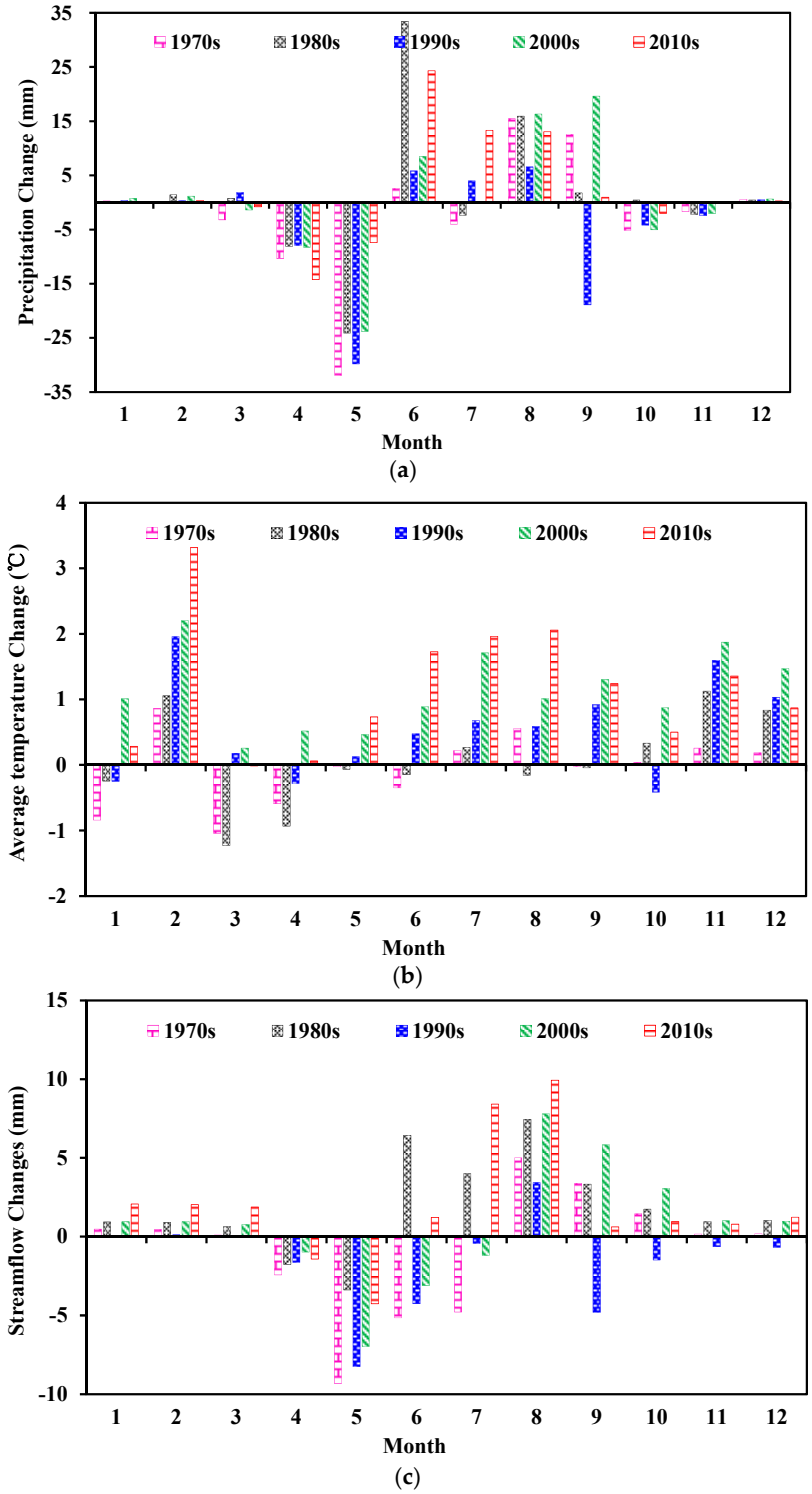

Figure 10. Decadal changes of monthly precipitation (**a**), average temperature (**b**), and streamflow (**c**) compare to the baseline of 1960s.

Generally, great changes have occurred from April to October, during which period the precipitation occupied over 90% of the total annual precipitation, and the streamflow count was 84% of total annual streamflow. Basically, the streamflow decreased from April to June for all five decades, except the streamflow increased in June during the 1980s and the 2010s. However, the streamflow is crucial to agricultural irrigation and stability of the oasis in the middle stream of Heihe River during

this period. The decreasing of streamflow might lead to grain reduction and oasis retreat. Meanwhile, the streamflow increased from August to October, except when the streamflow decreased in September and October during the 1990s. According to Figure 6, the peak of monthly streamflow occurred in July and August. The obvious increase of streamflow during this period could lead to the intensity of flood and high risks of hazards. Overall, climate change makes the intra-year distribution of streamflow more uneven. The climate streamflow–related potential risks have increased, consistent with the results of Zhang et al. [17]. In addition, the streamflow increased in almost all decades in the cold season from November to the following March. Over the last 50 years, the streamflow induced by climate change in the cold season increased 15.2 mm and in warm season (April to October) increase by 8.5 mm. The increasing of streamflow contributed to the increasing of total streamflow by 64.1% for cold season and 35.9% for warm season.

5. Conclusions

Understanding and quantifying the impacts of climate change and land cover change on hydrological response are of great significance for fine water resource management and planning in water-limited regions, especially in inland river basins. In this study, we employed the SWAT model to simulate the monthly streamflow of the upper reaches of Heihe River Basin over last 50 years. The simulation results were very satisfactory. Based on the simulation results, we calculated the contribution of climate change and land cover change to the streamflow increasing.

We concluded that the climate change and land cover change both contributed to the increase of the streamflow, whereas climate change was the main factor, consistent with the conclusions of several previous studies [17,36,53]. Because of the changes to climate and land cover, the rainfall-runoff relationship has varied, which has also been demonstrated in previous studies [1,31].

In this study, although the impacts of climate change and land cover change have been successfully examined, there is still room for improvement. For example, the uncertainty linked to the parameters should be quantified. All analyses done were based on only a chosen parameter; however, the hydrological response to different parameters can be different. Therefore, the parameter uncertainty should be tested in future.

This study can provide some references for dealing with climate change and land cover change in inland river basin water resource management and planning. As mentioned previously, millions of people are sustained by the streamflow of YLX watershed. This study shows a decreasing streamflow in the spring and increasing streamflow in the summer caused by changes of climate and land cover, which perhaps should push policymakers to change their water management planning [17].

Acknowledgments: This work was supported by the National Natural Science Foundation of China (Grant Nos. 41601038, 41571031), the Key Research Program of Frontier Sciences, CAS (QYZDJ-SSW-DQC031), the National Key R&D Plan (2017YFC0404302, 2016YFC0400908), the China Postdoctoral Science Foundation (Grant No. 2015M572620), and the Foundation for Excellent Youth Scholars of Northwest Institute of Eco-Environment and Resources, CAS. The authors would like to thank the anonymous reviewers for reading the manuscript and for their very valuable comments.

Author Contributions: Qi Feng designed this study; Zhenliang Yin and Linshan Yang prepared the driven data and set up the SWAT model; Xiaohu Wen and Songbing Zou contributed to calibrate the model; the manuscript was prepared by Zhenliang Yin, Qi Feng, and Linshan Yang, and revised by Jianhua Si and Xiaohu Wen.

Conflicts of Interest: The authors declare no conflict of interest.

References

1. Yang, D.; Gao, B.; Jiao, Y.; Lei, H.; Zhang, Y.; Yang, H.; Cong, Z. A distributed scheme developed for eco-hydrological modeling in the upper heihe river. *Sci. China Earth Sci.* **2014**, *58*, 36–45. [CrossRef]
2. Feng, Q.; Miao, Z.; Li, Z.; Li, J.; Si, J.; S, Y.; Chang, Z. Public perception of an ecological rehabilitation project in inland river basins in northern China: Success or failure. *Environ. Res.* **2015**, *139*, 20–30. [CrossRef] [PubMed]

3. Gao, G.; Fu, B.; Wang, S.; Liang, W.; Jiang, X. Determining the hydrological responses to climate variability and land use/cover change in the loess plateau with the budyko framework. *Sci. Total Environ.* **2016**, *557–558*, 331–342. [CrossRef] [PubMed]
4. Milly, P.C.; Dunne, K.A.; Vecchia, A.V. Global pattern of trends in streamflow and water availability in a changing climate. *Nature* **2005**, *438*, 347–350. [CrossRef] [PubMed]
5. Lopez-Moreno, J.I.; Zabalza, J.; Vicente-Serrano, S.M.; Revuelto, J.; Gilaberte, M.; Azorin-Molina, C.; Moran-Tejeda, E.; Garcia-Ruiz, J.M.; Tague, C. Impact of climate and land use change on water availability and reservoir management: Scenarios in the upper aragon river, Spanish pyrenees. *Sci. Total Environ.* **2014**, *493*, 1222–1231. [CrossRef] [PubMed]
6. Ye, X.; Zhang, Q.; Liu, J.; Li, X.; Xu, C.-Y. Distinguishing the relative impacts of climate change and human activities on variation of streamflow in the poyang lake catchment, China. *J. Hydrol.* **2013**, *494*, 83–95. [CrossRef]
7. Feng, Q.; Li, Z.; Liu, W.; Li, J.; Guo, X.; Wang, T. Relationship between large scale atmospheric circulation, temperature and precipitation in the extensive hexi region, China, 1960–2011. *Quat. Int.* **2016**, *392*, 187–196. [CrossRef]
8. Gu, X.; Zhang, Q.; Singh, V.P.; Chen, Y.D.; Shi, P. Temporal clustering of floods and impacts of climate indices in the tarim river basin, China. *Glob. Planet. Chang.* **2016**, *147*, 12–24. [CrossRef]
9. Tian, F.; Lü, Y.H.; Fu, B.J.; Yang, Y.H.; Qiu, G.; Zang, C.; Zhang, L. Effects of ecological engineering on water balance under two different vegetation scenarios in the Qilian mountain, northwestern China. *J. Hydrol. Reg. Stud.* **2016**, *5*, 324–335. [CrossRef]
10. Ning, T.; Li, Z.; Liu, W. Separating the impacts of climate change and land surface alteration on runoff reduction in the Jing River catchment of China. *Catena* **2016**, *147*, 80–86. [CrossRef]
11. Intergovernmental Panel on Climate Change. *Climate Change 2013: The Physical Science Basis*; IPCC: Cambridge, UK; New York, NY, USA, 2013.
12. Ponpang-Nga, P.; Techamahasaranont, J. Effects of climate and land use changes on water balance in upstream in the Chao Phraya River Basin, Thailand. *Agric. Nat. Resour.* **2016**, *50*, 310–320. [CrossRef]
13. Li, H.; Zhang, Y.; Vaze, J.; Wang, B. Separating effects of vegetation change and climate variability using hydrological modelling and sensitivity-based approaches. *J. Hydrol.* **2012**, *420*, 403–418. [CrossRef]
14. Falkenmark, M.; Rockstrom, J. *Balancing Water for Humans and Nature: The New Approach in Ecohydrology*; Routledge: London, UK, 2004.
15. DeFries, R.; Eshleman, K.N. Land-use change and hydrologic processes: A major focus for the future. *Hydrol. Process.* **2004**, *18*, 2183–2186. [CrossRef]
16. Tomer, M.D.; Schilling, K.E. A simple approach to distinguish land-use and climate-change effects on watershed hydrology. *J. Hydrol.* **2009**, *376*, 24–33. [CrossRef]
17. Zhang, L.; Nan, Z.; Yu, W.; Ge, Y. Modeling land-use and land-cover change and hydrological responses under consistent climate change scenarios in the Heihe River Basin, China. *Water Resour. Manag.* **2015**, *29*, 4701–4717. [CrossRef]
18. Dessu, S.B.; Melesse, A.M. Modelling the rainfall-runoff process of the mara river basin using the soil and water assessment tool. *Hydrol. Process.* **2012**, *26*, 4038–4049. [CrossRef]
19. Liu, Y.; Zhang, J.; Wang, G.; Liu, J.; He, R.; Wang, H.; Liu, C.; Jin, J. Quantifying uncertainty in catchment-scale runoff modeling under climate change (case of the Huaihe River, China). *Quat. Int.* **2012**, *282*, 130–136. [CrossRef]
20. Qin, J.; Ding, Y.; Wu, J.; Gao, M.; Yi, S.; Zhao, C.; Ye, B.; Li, M.; Wang, S. Understanding the impact of mountain landscapes on water balance in the Upper Heihe River watershed in northwestern China. *J. Arid Land* **2013**, *5*, 366–383. [CrossRef]
21. Xu, X.; Yang, D.; Yang, H.; Lei, H. Attribution analysis based on the budyko hypothesis for detecting the dominant cause of runoff decline in Haihe Basin. *J. Hydrol.* **2014**, *510*, 530–540. [CrossRef]
22. Wang, X. Advances in separating effects of climate variability and human activity on stream discharge: An overview. *Adv. Water Resour.* **2014**, *71*, 209–218. [CrossRef]
23. Zhao, A.; Zhu, X.; Liu, X.; Pan, Y.; Zuo, D. Impacts of land use change and climate variability on green and blue water resources in the Weihe River Basin of northwest China. *Catena* **2016**, *137*, 318–327. [CrossRef]
24. Yan, R.; Gao, J.; Li, L. Modeling the hydrological effects of climate and land use/cover changes in Chinese lowland polder using an improved walrus model. *Hydrol. Res.* **2016**, *47*, 84–101. [CrossRef]

25. Sarhadi, A.; Burn, D.H.; Johnson, F.; Mehrotra, R.; Sharma, A. Water resources climate change projections using supervised nonlinear and multivariate soft computing techniques. *J. Hydrol.* **2016**, *536*, 119–132. [CrossRef]
26. Chiarelli, D.D.; Davis, K.F.; Rulli, M.C.; D'Odorico, P. Climate change and large-scale land acquisitions in africa: Quantifying the future impact on acquired water resources. *Adv. Water Resour.* **2016**, *94*, 231–237. [CrossRef]
27. Zhang, L.; Podlasly, C.; Ren, Y.; Feger, K.-H.; Wang, Y.; Schwärzel, K. Separating the effects of changes in land management and climatic conditions on long-term streamflow trends analyzed for a small catchment in the loess plateau region, NW China. *Hydrol. Process.* **2014**, *28*, 1284–1293. [CrossRef]
28. Lu, Z.; Zou, S.; Xiao, H.; Zheng, C.; Yin, Z.; Wang, W. Comprehensive hydrologic calibration of SWAT and water balance analysis in mountainous watersheds in northwest China. *Phys. Chem. Earth Parts A/B/C* **2015**, *79–82*, 76–85. [CrossRef]
29. Geng, X.; Wang, X.; Yan, H.; Zhang, Q.; Jin, G. Land use/land cover change induced impacts on water supply service in the upper reach of Heihe River Basin. *Sustainability* **2014**, *7*, 366–383. [CrossRef]
30. Huang, G. From water-constrained to water-driven sustainable development—A case of water policy impact evaluation. *Sustainability* **2015**, *7*, 8950–8964. [CrossRef]
31. Yin, Z.; Feng, Q.; Zou, S.; Yang, L. Assessing variation in water balance components in Mountainous Inland River Basin experiencing climate change. *Water* **2016**, *8*, 472. [CrossRef]
32. Wu, F.; Zhan, J.; Wang, Z.; Zhang, Q. Streamflow variation due to glacier melting and climate change in Upstream Heihe River Basin, northwest China. *Phys. Chem. Earth Parts A/B/C* **2015**, *79–82*, 11–19. [CrossRef]
33. Zang, C.F.; Liu, J.; van der Velde, M.; Kraxner, F. Assessment of spatial and temporal patterns of green and blue water flows under natural conditions in Inland River Basins in northwest China. *Hydrol. Earth Syst. Sci.* **2012**, *16*, 2859–2870. [CrossRef]
34. Deng, X.; Shi, Q.; Zhang, Q.; Shi, C.; Yin, F. Impacts of land use and land cover changes on surface energy and water balance in the Heihe River Basin of China, 2000–2010. *Phys. Chem. Earth Parts A/B/C* **2015**, *79–82*, 2–10. [CrossRef]
35. Yin, Z.; Xiao, H.; Zou, S.; Zhu, R.; Lu, Z.; Lan, Y.; Shen, Y. Simulation of hydrological processes of mountainous watersheds in Inland River Basins: Taking the Heihe Mainstream River as an example. *J. Arid Land* **2013**, *6*, 16–26. [CrossRef]
36. Yang, L.; Feng, Q.; Yin, Z.; Wen, X.; Si, J.; Li, C.; Deo, R.C. Identifying separate impacts of climate and land use/cover change on hydrological processes in Upper Stream of Heihe River, northwest China. *Hydrol. Process.* **2017**, *31*, 1100–1112. [CrossRef]
37. Cheng, G.; Li, X.; Zhao, W.; Xu, Z.; Feng, Q.; Xiao, S.; Xiao, H. Integrated study of the water-ecosystem-economy in the Heihe River Basin. *Natl. Sci. Rev.* **2014**, *1*, 413–428. [CrossRef]
38. Chen, Y.; Deng, H.; Li, B.; Li, Z.; Xu, C. Abrupt change of temperature and precipitation extremes in the arid region of northwest China. *Quat. Int.* **2014**, *336*, 35–43. [CrossRef]
39. Li, B.; Chen, Y.; Shi, X. Why does the temperature rise faster in the arid region of northwest China? *J. Geophys. Res. Atmos.* **2012**, *117*, D16115. [CrossRef]
40. Wang, H.; Chen, Y.; Xun, S.; Lai, D.; Fan, Y.; Li, Z. Changes in daily climate extremes in the arid area of northwestern China. *Theor. Appl. Climatol.* **2012**, *112*, 15–28. [CrossRef]
41. Gao, Y.; Chen, F.; Barlage, M.; Liu, W.; Cheng, G.; Li, X.; Yu, Y.; Ran, Y.; Li, H.; Peng, H.; et al. Enhancement of land surface information and its impact on atmospheric modeling in the Heihe River Basin, northwest China. *J. Geophys. Res.* **2008**, *113*, D20S90. [CrossRef]
42. Arnold, J.G.; Srinivasan, R.; Williams, J.R. Large area hydrologic modeling and assessment. Part I: Model development. *J. Am. Water Resour. Assoc.* **1998**, *34*, 73–89. [CrossRef]
43. Neitsch, S.L.; Arnold, J.G.; Kiniry, J.R.; Williams, J.R. *Soil and Water Assessment Tool Theoretical Documentation (Version 2005)*; USDA-ARS Grassland, Soil and Water Research Laboratory: Temple, TX, USA, 2005.
44. Abbaspour, K.C. *SWAT-CUP, SWAT Calibration and Uncertainty Programs*; Swiss Federal Institute of Aquatic Science and Technology: Dübendorf, Switzerland, 2011.
45. Moriasi, D.N.; Arnold, J.G.; Van Liew, M.W.; Bingner, R.L.; Harmel, R.D.; Veith, T.L. Model evaluation guidelines for systematic quantification of accuracy in watershed simulations. *Trans. ASABE* **2007**, *50*, 885–900. [CrossRef]
46. Mann, H.B. Nonparametric tests against trend. *Econometrica* **1945**, *13*, 245–259. [CrossRef]

47. Kendall, M.G. *Rank Correlation Methods*; Griffin: London, UK, 1975.
48. Tesemma, Z.K.; Mohamed, Y.A.; Steenhuis, T.S. Trends in rainfall and runoff in the Blue Nile Basin: 1964–2003. *Hydrol. Process.* **2010**, *24*, 3747–3758. [CrossRef]
49. Hamed, K.H. Trend detection in hydrologic data: The mann-kendall trend test under the scaling hypothesis. *J. Hydrol.* **2008**, *349*, 350–363. [CrossRef]
50. Hamed, K.H.; Rao, A.R. A modified mann-kendall trend test for autocorrelated data. *J. Hydrol.* **1998**, *204*, 182–196. [CrossRef]
51. Sen, P.K. Estimates of the regression coefficient based on kendall's tau. *J. Am. Stat. Assoc.* **1968**, *63*, 1379–1389. [CrossRef]
52. Wu, F.; Zhan, J.; Chen, J.; He, C.; Zhang, Q. Water yield variation due to forestry change in the head-water area of Heihe River Basin, northwest China. *Adv. Meteorol.* **2015**, *2015*, 1–8. [CrossRef]
53. Wu, F.; Zhan, J.; Su, H.; Yan, H.; Ma, E. Scenario-based impact assessment of land use/cover and climate changes on watershed hydrology in Heihe River Basin of northwest China. *Adv. Meteorol.* **2015**, *2015*, 1–11. [CrossRef]